Mathematical modelling and active control of a buffet phenomenon

Alain Le Pourhiet [1], Michel Corrège [1], Daniel Caruana [2]

[1] Département Commande des Systèmes et Dynamique du vol (DCSD)
[2] Département Modèles pour l'Aérodynamique et l'Énergétique (DMAE)
ONERA, 2 av. Édouard Belin, 31400 Toulouse, France

e.mail : alain.le_pourhiet@cert.fr michel.correge@cert.fr daniel.caruana@onecert.fr

Summary - In order to obtain a mathematical model of two-dimensional buffet carried out in a wind tunnel, a Van der Pol oscillator has been enhanced with a transfer function identified from measurements. Using Control Engineering techniques, the above model was then used to define a control law aiming to suppress the buffet. On the experiment site, the effects of this law proved to conform to the theory, thus validating the principles of this type of modelling and design, and paving the way for this research to be applied in the three-dimensional field.

1 - Introduction

In the absence of precise explanations and of mathematical equations from physics laws to describe the buffet phenomenon, it seemed useful to find a simple mathematical model which could reproduce the observations obtained in the experiments and which could then be used, away from the experiment site, as a tool in the research into control laws. The Van der Pol oscillator is one of the most widely-studied oscillators in existence. It is particularly flexible, as all intervening parameters can be standardised. Tests were nevertheless made to ensure that this oscillator was representative. The simple second order Van der Pol oscillator was enhanced with transfer functions upstream and downstream, allowing the effects observed in the wind tunnel to be reproduced and a reliable mathematical model thus to be obtained.

Before studying the actual Van der Pol oscillator, we give a short presentation of the two types of oscillators in general use. This presentation leads to a better understanding of the principle which causes self-oscillation. The buffet control was based on this principle.

The test installation, the model and actuator used, and the aerodynamic characteristics of the different tests are described in detail in references [18-21]. An aerodynamic approach to the buffet phenomenon is also set out here. The following paragraph describes the physical and experimental approach and resumes the work done.

2 - Buffet : physical description and experiment results

In general, instability of flow on aircraft wings in certain flight conditions, can lead to the phenomenon known as buffet. This causes an unstationary flow separation which begins on the wing and couples with the wing to produce its own mode of vibrations on the structure (these modes can be different from aerodynamic instability modes). This phenomenon can appear in any flight condition. It is accentuated in transsonic flow by the movement of the position of the shock wave caused by the flow separations, when these spread from the shock to the trailing edge. It limits the flight envelope. It clearly appears necessary to delay the start of buffet in order to optimise the aircraft and its flight envelope. This study was carried out on two-dimensional flow.

2.1 - Description of the buffet phenomenon with shock wave in two-dimensional flow.

The transsonic flows are crossed by shock waves caused by a sudden recompression of the flow (fig. 1). These waves interfere with the boundary layer, an area of thick liquid near the wall. A complex, localised interaction occurs which deteriorates local distribution of speed until flow separation is formed. When the intensity of the shock wave is great enough, through increase of angle of attack for example, the flow separation spreads to the trailing edge and its level increases. Instabilities then develop on a large scale. The level of flow separation fluctuates with the position of the shock

wave, which moves from upstream to downstream and vice versa. The frequencies and amplitudes of the fluctuations depend on the dimensions of the wing and the aerodynamic conditions of the flow.

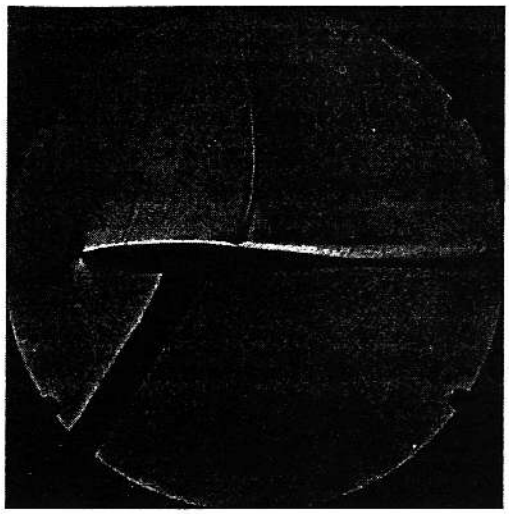

Figure 1 – Display of shock and flow separation by Schlieren photography.

The pressure levels, and therefore the lift, vary very greatly (fig. 2). These "aerodynamic instabilities" can be compared to oscillations and will hereafter be referred to as "buffet".

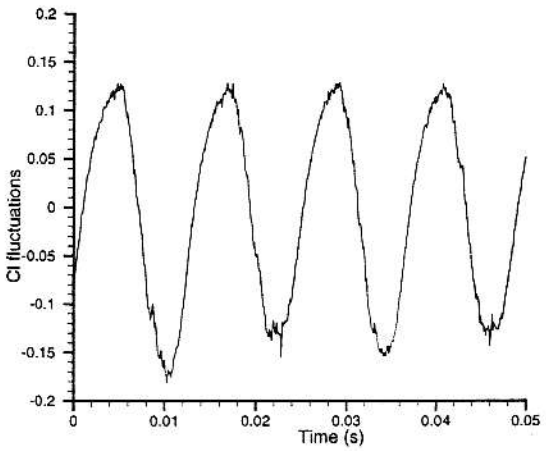

Figure 2 - Fluctuations in the lift coefficient..

2.2 - Wind tunnel tests.

These tests were carried out in the T2 wind tunnel of the DMAE department at ONERA Toulouse. It is a transsonic, pressurised, cryogenic wind tunnel with closed circuit (fig. 3). The instabilities studied are only aerodynamic (i.e. buffet). There was no vibration of the structure of the model, this being rigid and fixed to the walls of the test section.

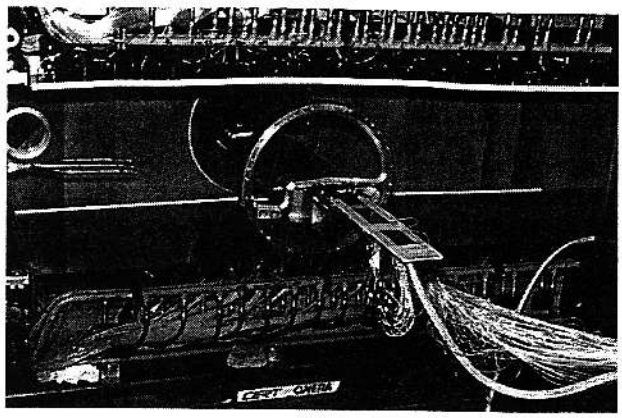

Figure 3 - The model in the wind tunnel test section.

2.2.1 - The model and its actuator.

After a bibliographical study, an "original" actuator was designed and developed. It is a new mobile part of the wing. Airfoil OAT15A was chosen. The model is 200mm wing chord and is equipped with 68 fixed static pressure points and 19 unsteady static pressure points (fig. 4). The measurements were carried out simultaneously at a sampling rate of 15000 points per second and with a filtered signal of 5000Hz.

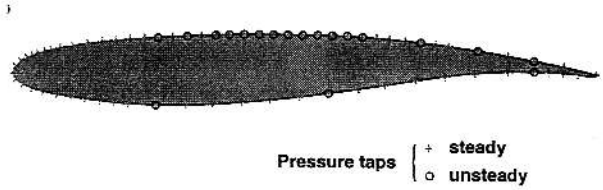

Figure 4 - The OAT15A wing section and instrumentation of the model.

2.2.2 - Mobile results.

The start of buffet corresponds to an increase in the pressure fluctuations measured on the wing upper and lower surfaces (fig. 5).

During buffet conditions, the signals measured are near-periodical. A peak, characteristic of buffet in two-dimensional flow, can be observed on the spectrum (fig. 6). Its frequency depends on the dimensions of the wing section and on the conditions of flow.

The mobile position of the shock can be deduced from the pressure measurements (fig. 7). Various actuator controls in open loop (sinusoids, gaps, phase shifts, etc.) were tested to try to understand the aerodynamic effect of the actuator with and without buffet. In unstable cases, it was impossible to obtain a permanent stabilisation of the flow ; only transients realised with induced phase shifts (actuator/shock position) resulted in a short stabilisation of the flow.

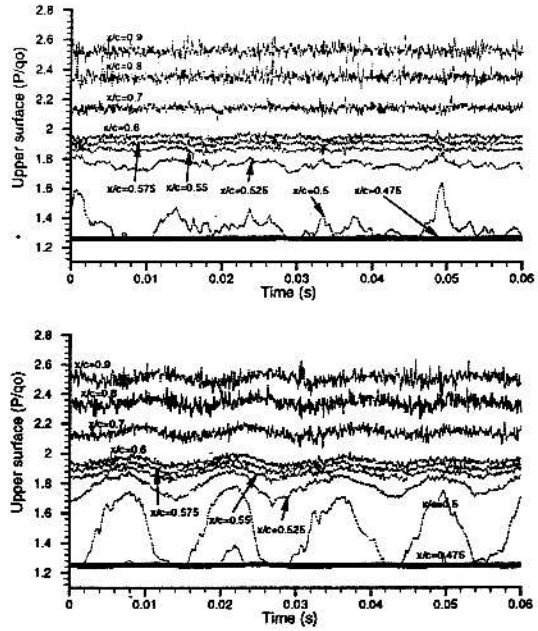

Figure 5 - Pressure fluctuations before and after buffet onset.

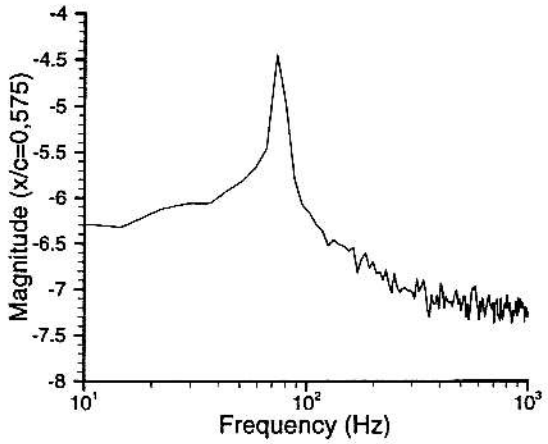

Figure 6 - Spectrum of the signal from a pressure sensor located at the shock location.

In open loop with sine-shaped control signals, the oscillation of the shock tends to become stronger and to take its frequency from the actuator. It thus causes buffet from certain amplitudes and frequencies of its movement (fig. 8). These observations are useful in the mathematical modelling of the phenomenon, since they also characterise the Van der Pol oscillators, as shall be seen later.

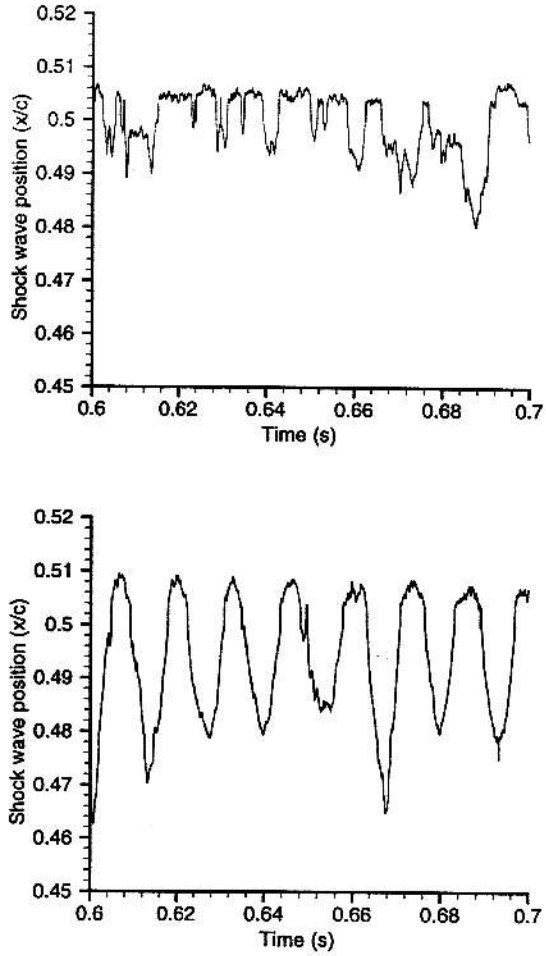

Figure 7 - Mobile position of the shock just before and just after start of buffet.

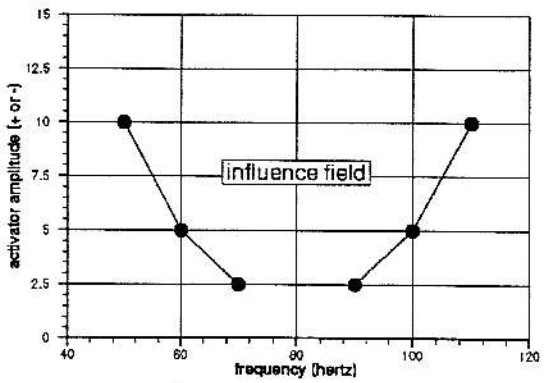

Figure 8 - Field of influence of the actuator on buffet.

Flow could only be stabilised with a closed loop approach, based on the unsteady measurement of the distribution of static pressure on the wing section (fig. 9).

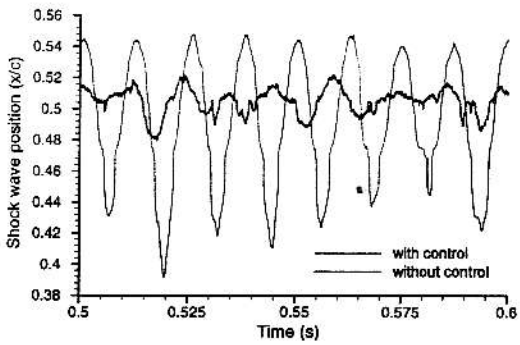

Figure 9 - Active control of buffet in closed loop. Mobile position of the shock. See also figure 23.

Flow on the wing section is stabilised. The fluctuations of the position of the shock, and thus those of the airfoil section lift, are clearly diminished. The control law used to obtain this result (its structure and parameters) was first determined empirically during the tests, then confirmed qualitatively and quantitatively by the theoretical study which follows.

3 - On the general principles of oscillators

3.1 - Condition required for self-oscillation

Let us consider the system

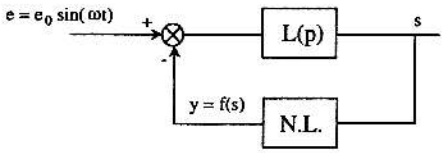

Figure 10 - Linear system closed with non-linearity

in which y = f(s) is a non-linear function of the output s and p is the Laplace operator, i.e. the symbol of derivation in relation to time. It corresponds to the equation

$$[L(p)]^{-1}s + f(s) = e_0 \sin\omega t \qquad (1)$$

It is assumed that the transfer function L(p) efficiently filters the harmonics above the fundamental ω, thus allowing them to be ignored. We thus have, in established sinusoidal conditions,

$$s = s_0 \sin(\omega t + \varphi) \qquad (2)$$

with

$$\frac{s_0}{e_0} e^{j\varphi} = \frac{L(j\omega)}{1 + N(s_0,\omega)L(j\omega)} \qquad (3)$$

in which $N(s_0,\omega)$ is the harmonic equivalent gain of the non-linearity ; it depends on s_0, and eventually on ω if derivatives of s appear in f(s) ; it is complex when there is a phase shift between y and s. If the system is the site of a self-oscillation when $e_0 = 0$, we must have

$$1 + N(s_0,\omega)L(j\omega) = 0$$

thus

$$L(j\omega) = -\frac{1}{N(s_0,\omega)}. \qquad (4)$$

In the complex plane, $-1/N(s_0,\omega)$, for each frequency ω, is the "critical locus" of the non-linearity, graduated in s_0. One condition required for self-oscillation to exist is that there be a couple (s_0, ω_0) intersection of the Nyquist locus $L(j\omega)$ with one of the critical locus. Following this, it is supposed that the harmonic equivalent gain does not depend on ω, and we therefore refer to one critical locus only. Self-oscillation really exists provided that it is stable.

3.2 - Conditions of stability

Let us write s and f(s) as

$$s = s_0 \sin(\omega t + \varphi) = X \sin\omega t + Y \cos\omega t,$$
$$f(s) = q_1(X,Y)\sin\omega t + q_2(X,Y)\cos\omega t.$$

The identification of the terms in sin(ωt) and cos(ωt) in the two members of (1) leads to (ref.[1-3])

$$e^{T p u} M Z + \begin{bmatrix} q_1(X,Y) \\ q_2(X,Y) \end{bmatrix} = \begin{bmatrix} e_0 \\ 0 \end{bmatrix} \qquad (5)$$

where

$$T = \frac{d}{d\omega},\ p = \frac{d}{dt},\ u = \begin{bmatrix} 0 & 1 \\ -1 & 0 \end{bmatrix},\ M = \begin{bmatrix} R(\omega) & -I(\omega) \\ I(\omega) & R(\omega) \end{bmatrix},\ Z = \begin{bmatrix} X \\ Y \end{bmatrix},$$

$R(\omega)$ and $I(\omega)$ being the real and imaginary parts of $[L(j\omega)]^{-1}$. The balance is obtained by the operation p = 0 in (5), i.e.

$$M Z_0 + \begin{bmatrix} q_1(X_0,Y_0) \\ q2(X_0,Y_0) \end{bmatrix} = \begin{bmatrix} e_0 \\ 0 \end{bmatrix}. \qquad (6)$$

The solutions to (6) give the descriptive ordinates (X_0, Y_0) of the oscillation. Let us consider a small perturbation dZ around Z_0. We have

$$\left[e^{T p u} M + J_0\right] dZ = 0 \qquad (7)$$

with

$$J_0 = \begin{bmatrix} \frac{\partial q_1}{\partial X} & \frac{\partial q_1}{\partial Y} \\ \frac{\partial q_2}{\partial X} & \frac{\partial q_2}{\partial Y} \end{bmatrix}_{(X=X_0, Y=Y_0)}$$

The stability of the oscillation (X_0, Y_0) depends on the roots of the characteristic polynomial

$$P(p) = \det\left[e^{Tpu}M + J_0\right] = \alpha_0 + \alpha_1 p + \alpha_2 p^2 + \ldots \qquad (8)$$

obtained by breaking down the matrix e^{Tpu} into a serie. The roots of this polynomial must have a negative real part. It must therefore be verified that the Routh-Hurwitz criterion applies to the α_i coefficients : these in particular must be of the same sign, in this case positive ; although this partial condition is only necessary, we shall consider it sufficient. It can be shown (ref. [1] and [2]) that

1) the required condition for stability $\alpha_0 > 0$ can be written

$$R^2 + I^2 + \xi_0 R - \eta_0 I + \det(J_0) \geq 0 \qquad (9)$$

with

$$\zeta_0 = \left(\frac{\partial q_1}{\partial X} + \frac{\partial q_2}{\partial Y}\right)_0, \quad \eta_0 = \left(\frac{\partial q_1}{\partial Y} - \frac{\partial q_2}{\partial X}\right)_0,$$

the 0 index signifying that the derivatives are taken from the solution to (6). It excludes solutions such as $(ds_0/d\omega) < 0$, i.e. those solutions included between two vertical tangent points of the curve $s_0(\omega)$. It also explains the jumps in amplitude of s observed when proceeding at increasing or decreasing frequency for a constant amplitude e_0 (ref. [1] to [4]).

2) In the specific case of self-oscillation ($e_0 = 0$), the required condition of stability $\alpha_1 > 0$ is written

$$\frac{dI}{d\omega}(2R + \xi_0) - \frac{dR}{d\omega}(2I + \eta_0) \geq 0. \qquad (10)$$

It is expressed thus : *when examining the Nyquist locus L(jω) in the direction of the increasing frequencies, on the left is the direction of the increasing s_0 on the critical locus -1/N(s_0) at their intersection.* In this way, two types of oscillators are defined :

-type A : those whose harmonic equivalent gain of non-linearity decreases with s_0 ;

-type B : those where it decreases with s_0.

One example of type A is given by the stable transfer function

$$L_A(p) = p/(p^2 + 2z\omega_0 p + \omega_0^2)$$

associated to the non-linearity f(s) = k*sign(s) whose harmonic gain is $N_A(S_0) = 4k/(\pi s_0)$. The critical locus is on the negative real half-axis. A stable self-oscillation thus exists, of ω_0 frequency and of amplitude

$$s_0 = -(4k/\pi)\mathrm{Re}[L_A(j\omega_0)] = 2k/(\pi z\omega_0).$$

This type of oscillation is seen in controls showing saturation of control ; it is then a parasite phenomenon well known in control engineering [4].

One example of type B (see figure 12) is given by the unstable linear part

$$L_B(p) = p/(p^2 - 2z\omega_0 p + \omega_0^2)$$

associated to the cubic function $f(s) = ks^3$ whose harmonic gain is

$$N_B(s_0) = 0.75\,k\,s_0^2 . \qquad (11)$$

The critical locus $-1/N_B(s_0)$ is once again on the real negative axis. The stable oscillation is of frequency ω_0 and of amplitude

$$s_0 = \sqrt{\frac{-4}{3k\,\mathrm{Re}\left[L_B(j\omega_0)\right]}} = \sqrt{\frac{8z\omega_0}{3k}} . \qquad (12)$$

This oscillator is known as a "Van der Pol". It is often seen in physics, particularly in electronic circuits.

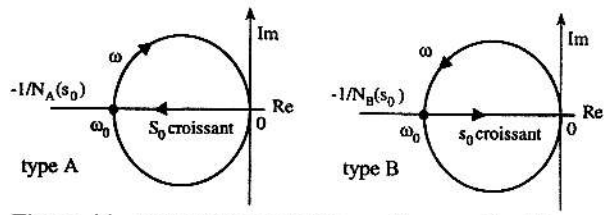

Figure 11 - Nyquist locus and non-linear critical locus for A- and B-type oscillators.

Notes

1) In the phase plane (s',s) these self-oscillations correspond to stable limit cycles, which have been analysed in many studies [4-16]

2) For the cubic non-linearity we have

$$(\sin\omega t)^3 = 0.75\sin\omega t - 0.25\sin 3\omega t .$$

The third harmonic has an amplitude three times smaller than the first harmonic. In general, it is attenuated even more by the linear filter L(p) and this reinforces the approximation of the first harmonic on which everything we have said so far is based.

4 - The Van der Pol oscillator

Of the two oscillators described earlier, we chose the second to represent buffet. Indeed, as far as we know at present, it is more likely to correspond to the observed reality, because of its description of numerous natural phenomena. Thus the Van der Pol equation :

$$\ddot{s} - 2z\omega_0\dot{s} + \omega_0^2 s + 3ks^2\dot{s} = e_0\,\omega\cos\omega t \qquad (13)$$

is equivalent to the system in figure 12.

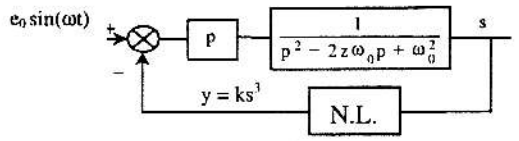

ω : pulsation ; k : gain ; z : amortissement.

Figure 12 - Block diagram of a Van der Pol oscillator.

If we write s as $s = X \sin \omega t + Y \cos \omega t$, and we put this expression into (13), we find (ref. [3], [5] to [17])

$$\rho\left[\sigma^2 + (\rho - 1)^2\right] = F^2 \tag{14}$$

with the standardised parameters

$$\rho = \frac{3k}{8z\omega_0}\left(X^2 + Y^2\right), \tag{15}$$

$$F^2 = \frac{3ke_0^2}{32z^3\omega_0^3}, \tag{16}$$

$$\sigma = \frac{\omega^2 - \omega_0^2}{2z\omega\,\omega_0}. \tag{17}$$

The conditions of stability $\alpha_0 > 0$ and $\alpha_1 > 0$ given by the above method can be written respectively

$$(3\rho - 1)(\rho - 1) + \sigma^2 > 0 \tag{18}$$

and

$$\rho > 0.5\,. \tag{19}$$

The ellipse $(3\rho - 1)(\rho - 1) + \sigma^2 = 0$ is the locus of the points with vertical tangents of the curves $\rho(\sigma)$ for all the F^2 (see figure 13). The condition $\alpha_0 > 0$ thus expresses the "saddle instability" inside this "jump" ellipse. The condition $\rho > 0.5$ excludes unstable focus that are due to the presence of a residual self-oscillation of ω_0 frequency ; this is visible in time simulation by a modulation of the amplitude at the frequency ω-ω_0 ; in the (Y,X) plane we have a limit cycle at frequency ω_0. For more details about the kinds of instability see references [6-17]. Clearly, since ρ is an increasing function of F^2, the condition $\rho > 0.5$ expresses the existence of a threshold for F^2 (and thus for e_0) below which the frequency oscillation ω cannot appear alone, its amplitude and frequency remaining confused by the self-oscillation signal (see figure 17). Above this threshold, the $\bullet_0$ frequency is muffled and only the ω frequency remains. The synchronisation threshold e_{0c} is obtained by effectuating $\rho = 0.5$ in (14) :

$$F_c^2 = 0.5\,(\sigma^2 + 0.25)\,, \tag{20}$$

then by carrying this value over into (16) :

$$e_{0c} = \frac{2}{\omega}\sqrt{\frac{z\omega_0}{3k}\left[\omega^4 + \omega_0^4 - \omega^2\,\omega_0^2\left(2 - z^2\right)\right]}\,. \tag{21}$$

e_{0c} is only defined for the right-hand part $\rho = 0.5$ outside the jump ellipse, i.e. approximately for $\sigma > 0.5$. The amplitude of the self-oscillation ($\sigma = 0$, $F^2 = 0$) corresponds to $\rho = 1$, i.e. according to (15)

$$s_0 = \sqrt{X^2 + Y^2} = \sqrt{\frac{8z\omega_0}{3k}}\,. \tag{22}$$

We indeed find relation (12). In figure 13 the response curves $\rho(\sigma)$ were plotted for different values of F^2. The value 4/27 is the limit below which the curve splits into two parts. The value 8/27 is the limit above which there are no points with vertical tangent.

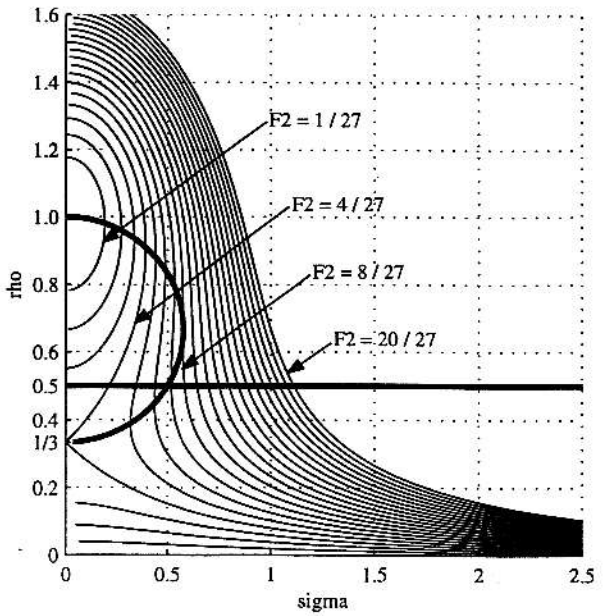

Figure 13 - Van der Pol oscillator : standardised output amplitude (ρ) vs σ and F^2.

In figure 14, e_{0c} is plotted vs the frequency for the values of z/k and z close to those which shall be chosen later. When the right-hand $\rho = 0.5$ is inside the jump ellipse ($\alpha_0 < 0$), oscillation is unstable, and the calculation of the synchronisation threshold is made using the equation of the part of this ellipse such as $\alpha_1 > 0$ (i.e. $\rho > 0.5$), instead of using $\rho = 0.5$. This explains the discontinuities in the curve at around $\omega = \omega_0$. The threshold for $\omega = \omega_0$ (self sustained oscillation) is obviously zero. Generally speaking, the synchronisation threshold is obtained by combining (6) with the equality (10), or with the equality (9) if the corresponding inequality has more constraints than (10). There is a remarkable similarity between the theoretical figure 14 and the experimental figure 8.

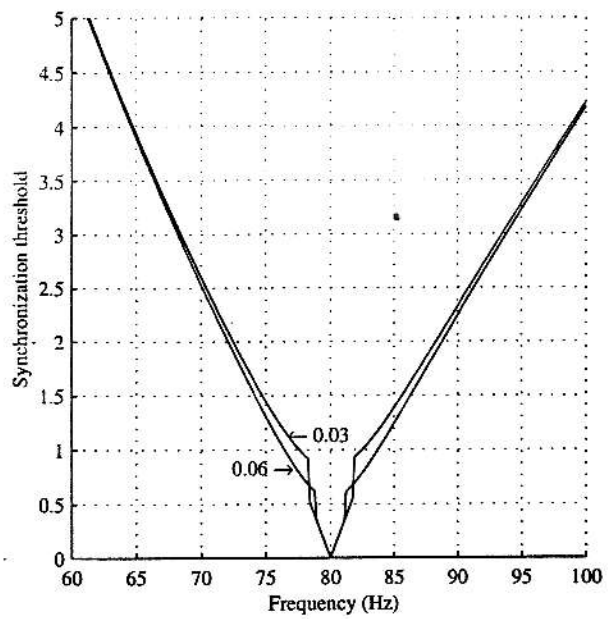

Figure 14 - Van der Pol oscillator (z/k = 5 10^{-7}) : synchronisation threshold vs frequency for z = 0.03 and z = 0.06.

5 - Mathematical modelling the buffet

In figure 15 we have traced the 15 available tests carried out at frequencies of 60, 70, 80, 90 and 100 Hz. And for e_0 amplitudes of 2.5, 5 and 10. Whatever the frequency, the synchronisation threshold is always within the 2.5 to 5 range. Below this threshold, modulation is observed with both ω_0 and ω frequencies. We also have free tests ($e_0 = 0$) for which the system is self-oscillating at a frequency of 80 Hz. It is this self-oscillation (i.e. the buffet) which we aim to eliminate in this study.

To find a mathematical model of buffet, let us consider a Van der Pol oscillator equipped with transfert functions F_1 and F_2 that can suitably express the physical reality observed :

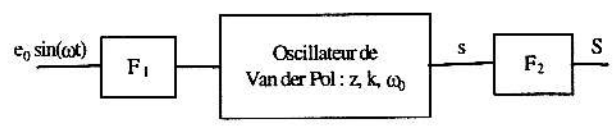

Figure 16 – Mathematical model of the buffet

F_1 and F_2, as well as the internal parameters of the oscillator (z and k), shall be identified from the experimental observations. The value of ω_0 is obviously 80 Hz. The F_1 function, upstream of the oscillator, must enable us to adjust the synchronisation on the roughly-measured threshold. The F_2 function, downstream, enables the amplitude and phase of the output S to be adjusted so that they coincide as well as possible with the measurements made for different ω and e_0. The frequency response of the mathematical model shall thus correspond to the experimental reality, and the conformity of the time responses may thus be deduced.

Particularly for 70 Hz and $e_0 = 2.5$ (see figure 17) the modulation observed is characteristic of a little damped system. The damping coefficient z of the oscillator is confirmed as being about 0.03.

The theoretical synchronisation threshold was plotted according to the frequency in figure 14. It mainly depends on the z/k parameter through the relationship (21) and little on z in the range ($z < 0.1$) that interests us. The best approach is obtained for $z/k = 5\ 10^{-7}$, although it is not possible to obtain an exact reproduction of the experimental synchronisation thresholds in the 2.5 to 5 range for all frequencies. To do so, the input would have to be multiplied by the following upstream gains :

Frequency (Hz)	60	70	80	90	100
Upstream gain	1.2	0.8	/	0.8	/

(they are neutral at 80 and 100 Hz). These gains would be easily produced by an F_1 transfer function. Unfortunately, when F_1 is introduced, its phase shift makes it is impossible to identify the downstream transfer function F_2. On the synchronisation thresholds we therefore have to accept a 20% error made by taking $F_1 = 1$, and consider whether the oscillator block needs to be improved by adjusting its linear part L(p) or its non-linearity f(s).

Even so, this is not of the utmost importance since we hope that this systematic error will later be absorbed by sufficient safety margins, when the control is developed further.

For the given values of e_0, z and ω (and thus of F^2), the calculation of the standardised amplitude ρ at the oscillator output is made by solving (14). If there is more than one real root, we retain only the largest ; from it we deduce s_0 by (15), then $g = s_0/e_0$, then the phase of s by the relationship (3) which is written here

$$g e^{j\varphi} = \frac{L(j\omega)}{1 + 0.75\, k\, s_0^2 L(j\omega)} \quad ; \qquad (23)$$

the gain of F_2 is then deduced from the measured gain S_0/e_0 by dividing it by g ; the phase of F_2 is deduced by subtracting φ from the measured phase of S. Using a suitable programme we go on to identify the coefficients of the numerator and the denominator of F_2 :

$$F_2(p) = \frac{1.45\ 10^1\, p^3 - 7.35\ 10^2\, p^2 + 3.29\ 10^6\, p - 6.76\ 10^8}{p^3 + 5.20\ 10^3\, p^2 + 1.09\ 10^6\, p + 9.26\ 10^8}.$$

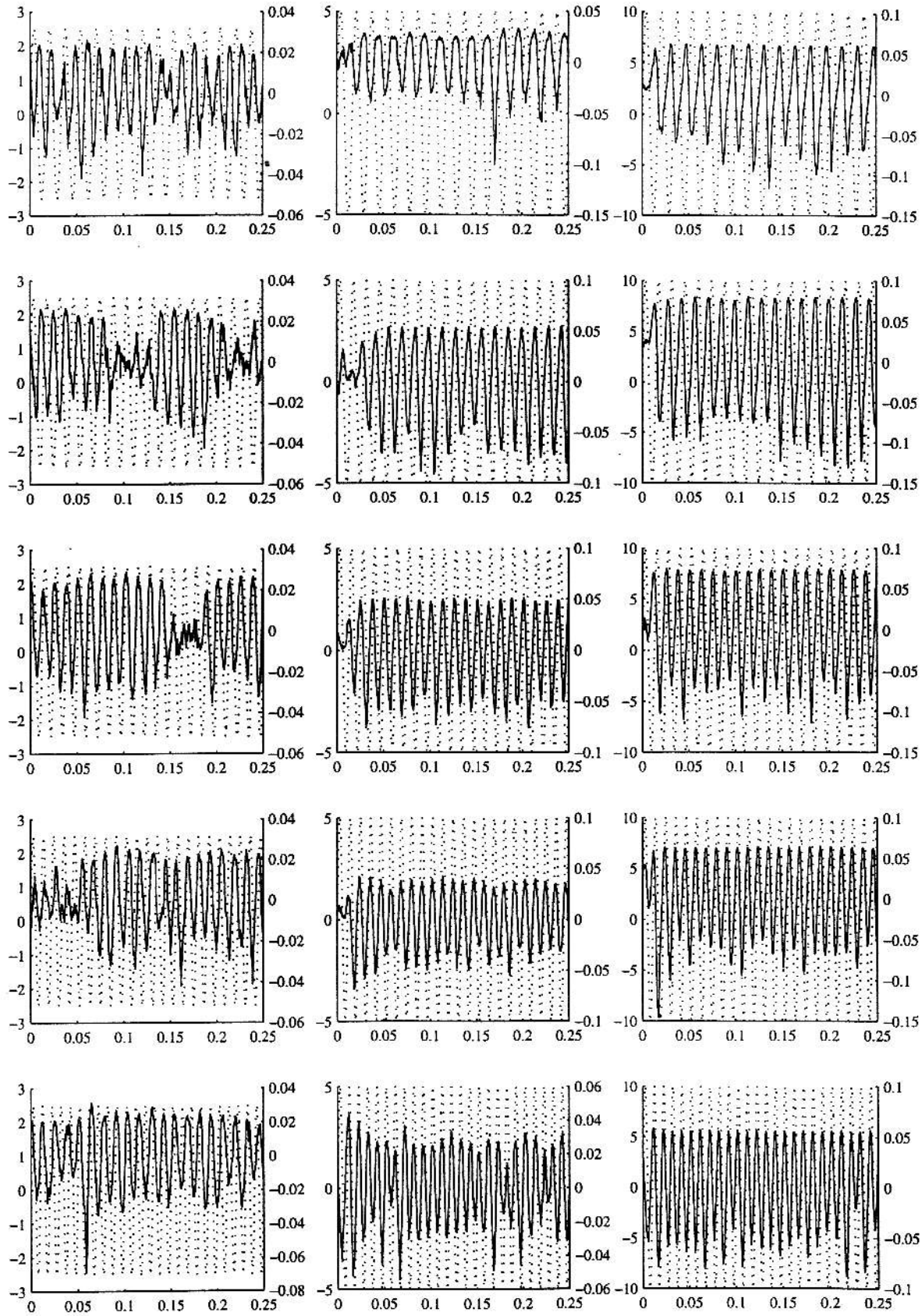

Figure 15 - Measured output signal (solid line, right-hand scale) and input sine signal (dotted line, left-hand scale). From left to right : e_0 = 2.5, 5 and 10. From top to bottom : frequency = 60, 70, 80, 90 and 100 Hz

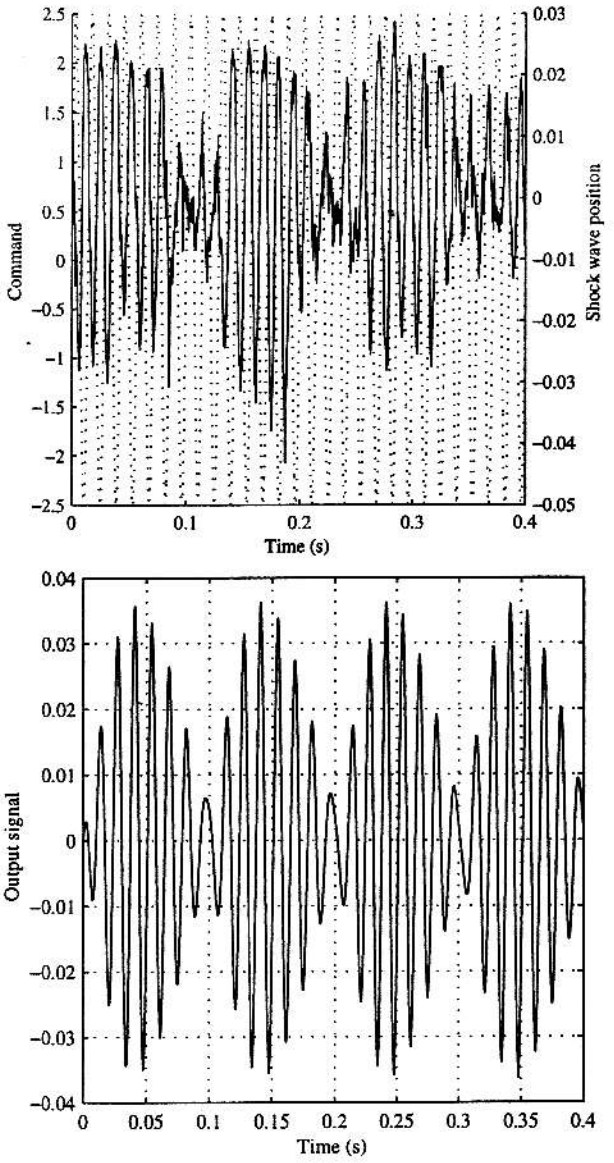

Figure 17 - Modulation observed at 70 Hz for $e_0 = 2.5$ and reproduced in simulation for $e_0 = 2$ (in order to make allowance for the 0.8 gain which should have been supplied by F_1).

The roots of the denominator have negative real part since we identify an obviously stable system ; some roots of the numerator have positive real part, and this is important to what follows. The curves in figure 18 give the gain and the phase of $F_2(j\omega)$ vs ω.

Notes -

1) The z/k ratio of the oscillator was determined at the same time as the identification of F_2, so that the theoretical amplitude of the oscillations would be equal to the measured amplitude (= 0.023). The relationship (22) gives

$$\frac{z}{k} = \frac{3}{8\omega_0}\left[\frac{0.023}{|F_2(j\omega_0)|}\right]^2 = 5\,10^{-7} .$$

It is satisfying to observe that this value was already the "least bad" to express the synchronisation threshold. Having chosen z = 0.027 because of the modulation shape, we thus find k = 54000.

2) In figure 18, we check that the gain and phase curves of $F_2(j\omega)$ run as they should between the points corresponding to $e_0 = 5$ and $e_0 = 10$ (the tests corresponding to $e_0 = 2.5$ are excluded from the identification as the output is not yet synchronised with the input). But these two families of points should in fact intermingle, since F_2 is linear and unique. If they do not intermingle, it is because the gain and phase of the theoretical oscillator have a non-linear dependency on the input which is different from that of the real oscillator ; after dividing the gains and subtracting the phases for the frequency definition of F_2, this difference remains. Although the present result is fairly satisfactory, it may be necessary to modify the oscillator — L(p) and f(s) — in order to minimise this difference and to make the mathematical model more representative of the physical reality.

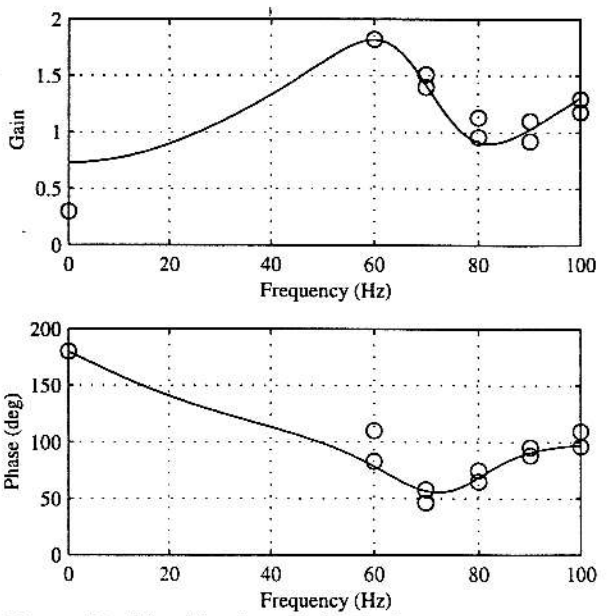

Figure 18 - Identification of the F_2 frequency response.

6 - Synthesis of the control law

6.1 - Principle

With no input, the system is the site of a self-oscillation which we aim to suppress with a feedback transfer function G :

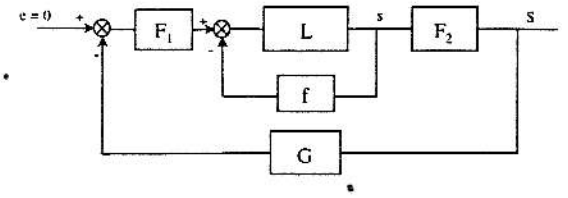

Figure 19 - System looped in feedback by a transfer function G aimed at controlling the buffet.

The overall transfer is

$$\frac{S}{e} = \frac{F_1 \dfrac{L}{1+N(s_0)L} F_2}{1+GF_1 \dfrac{L}{1+N(s_0)L} F_2}$$

$$= F_1 \frac{\Phi}{1+N(s_0)\Phi} F_2$$

where it is seen that

$$\Phi = \frac{L}{1+GLF_1F_2}, \qquad (24)$$

$N(s_0)$ being the equivalent harmonic gain of f(s). Everything happens as if it were no longer L(p), but the transfer function $\Phi(p)$, which was with the negative feedback f(s) :

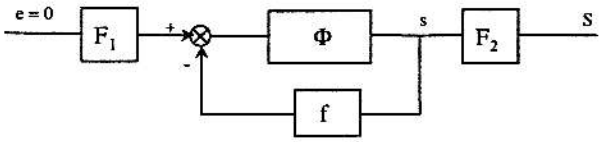

Figure 20 - Diagram equivalent to that in figure 16.

To muffle the oscillation, it is thus sufficient to choose G carefully, so that the oscillator can be made to no longer resemble a possible type-B oscillator as defined earlier. The relationship (24) is written

$$G = \frac{L-\Phi}{\Phi L F_1 F_2}. \qquad (25)$$

Following this we put

$$F_1 F_2 = C$$

(it is to be remembered that a particular approximation $F_1 = 1$ is being made here). If we associate their descriptive natural indices with the numerators and denominators of L, Φ and C, (25) becomes

$$\frac{N_G}{D_G} = \frac{N_L D_\Phi - D_L N_\Phi}{N_\Phi N_C N_L} D_C \cdot \qquad (26)$$

We put also

$$\alpha\beta = N_C N_L$$

where we concentrated in α the unstable (and eventually equal to zero) roots of $N_C N_L$ which must be simplified in (26) so that G is stable — it is not essential to impose stability for G, but it is a safety measure. If simplification is possible, there exist two polynomials P_1 and P_2 such that

$$(N_L D_\Phi - D_L N_\Phi) P_1 = \alpha N_\Phi P_2 \cdot \qquad (27)$$

We then have

$$\frac{N_G}{D_G} = \frac{D_C P_2}{\beta P_1} \qquad (28)$$

and

$$\frac{N_\Phi}{D_\Phi} = \frac{N_L P_1}{\alpha P_2 + D_L P_1} \cdot \qquad (29)$$

The following constraints are imposed for P_1 and P_2:

1) P_1 stable, so that G is stable ;

2) $\deg(N_G) \le \deg(D_G)$ so that the transfer G is physically possible ; this is written

$$\deg(P_1) - \deg(P_2) \ge \deg(D_C) - \deg(\beta). \qquad (30)$$

3) Finally, since the aim of this study is to eliminate the self-oscillation, the functions P_1 and P_2 shall be such that the Nyquist locus of $\Phi(j\omega)$, which defines the new equivalent oscillator, shall never cut the negative part of the real axis, on which the non-linear critical locus - $1/N(s_0)$ is situated. In other words, the phase of $\Phi(j\omega)$ must never be equal to π, whatever the frequency. One sufficient condition for the phase of a transfer function never to equal π is that this function be stable (i.e. no root of the denominator should have positive real part) and that the difference between the degrees of the denominator and the numerator does not exceed 2. Taking into account this constraint of difference in degrees, the following fundamental result can be given : *a necessary and sufficient condition for self-oscillation not to exist is that the transfer function Φ be stable.*

From (29) we now only need to find P_1 and P_2 so that the roots of $\alpha P_2 + D_L P_1$ have negative real part. One way to obtain this is by writing

$$P_2 = \beta P_2' \quad \text{et} \quad P_1 = D_C P_1' ;$$

(28) then gives :

$$\frac{N_G}{D_G} = \frac{P_2'}{P_1'}.$$

The G function can thus been found of low degree, improving following experimentation.

6.2 - Robustness to parameter errors

It has been seen that the robustness to the non-existence of self-oscillation is equivalent to that of the stability of Φ, i.e. equivalent to that of the GLC system looped in feedback by a unit gain. This robustness is expressed quantitatively from the stability margins of this system. On the Black locus of the GLC (gain vs phase) figures 21 and 22 show that the critical point ($\pm$ 180°, 0 db) is surrounded by a loop ; for the system to be stable, this loop has to surround the critical point, leaving it to the right when the locus is crossed in the direction of the increasing frequencies [5]. When there are unknown parasite gains and phases, the critical point must remain inside the loop. is well in the centre of the loop. Obviously, the best insurance in stability is obtained when the critical point is well in the centre of the loop. During the development of numerous G functions, we made particular effort to make both gain margins and both phase margins equal. It is easy to obtain approximately $\pm$15 db for the gain and $\pm$60° for the phase, which is perfectly convenient. In particular, such margins largely absorb the 20% error on the gain arising systematically when $F_1 = 1$.

6.3 - Results

Of all the numerous controls found (including a simple integrator) the two results below are particularly efficient :

1)

$$G_1 = \frac{4.81\,10^7 p^2 + 8.72\,10^9 p + 8.86\,10^{12}}{p^4 + 8.88\,10^2 p^3 + 4.79\,10^5 p^2 + 2.07\,10^8 p + 3.18\,10^{10}}$$

To figure 21 we give the Bode locus of G_1, the Black locus of LG_1C, and a time simulation. The time simulation shows the instability of the Van der Pol oscillator at zero (due to the negative damping of its linear part), followed by the appearance of oscillation which expresses an overall stability due to the positive damping caused by the non-linearity at high amplitudes. We apply control G_1 at moment 0.7 seconds ; the self-oscillation is then immediately and spectacularly muffled.

2) $\quad G_2 = 95 e^{-0.2 T_0 p} \qquad (T_0 = 2\pi / \omega_0)$

By its expansion (Padé approximation), this control by pure delay is equivalent to a rational fraction respecting the imposed constraints. The results are given in figure 22. This was the first control chosen to be set up on the experiment site in the wind tunnel. Figure 23 shows two real developments : the self-oscillation before application of control G_2, and the residue measured afterwards. The frequency analysis of these two signals is also shown, as well as the control time signal. These experiment results correspond extremely well to those predicted by the theory (see also figure 9).

6.4 - Robustness to disturbances

The mathematical model is a convenient assembly of two parts, the oscillator and the identified transfer function F_2 ; it is not possible to consider any internal disturbance which may occur, without greater study of the physical reality of this model.

As preparation for further study of robustness, we considered input noise only. For an output amplitude S equal to 0.02 (the amount of amplitude which interests us here), figure 24 gives the gains of the system looped by functions G_1 and G_2, for the frequency range 40-120 Hz ; gains are also given for no loop (G = 0). It can be seen that the damping around the resonance is by far the best with the function G_1. This is quite normal, since G_1 is of degree 2 over 4 which guarantees a filtering that does not exist with the pure delay G_2, whose gain, always equal to 95, is independent of the frequency.

7 - Conclusions

This study used a realistic mathematical model identified from measurements carried out in a wind tunnel, and including a Van der Pol oscillator. It led to the synthesis of a control which successfully muffles the buffet phenomenon. Modifications to the model may be made during future stages of the research if these modifications enable the model to improve the definition of synchronisation thresholds (defined with a 20% error margin) ; and also to improve definition of the non-linearity itself, as there is still some evidence of its weaknesses upstream. All things considered, the results obtained in this study are most encouraging ; they will form the basis of more complex research into the three-dimensional phenomenon which occurs on aircraft wings.

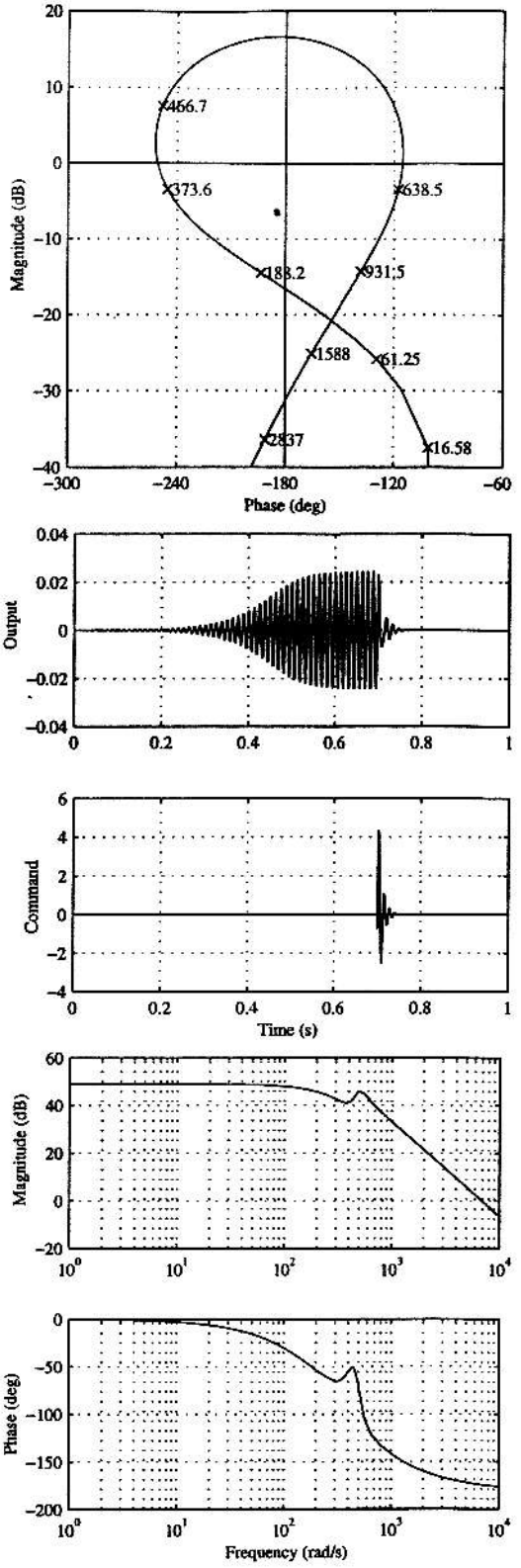

Figure 21 - Control function G_1. Black locus of LG_1C ; output and buffet suppression signals ; Bode locus of G_1.

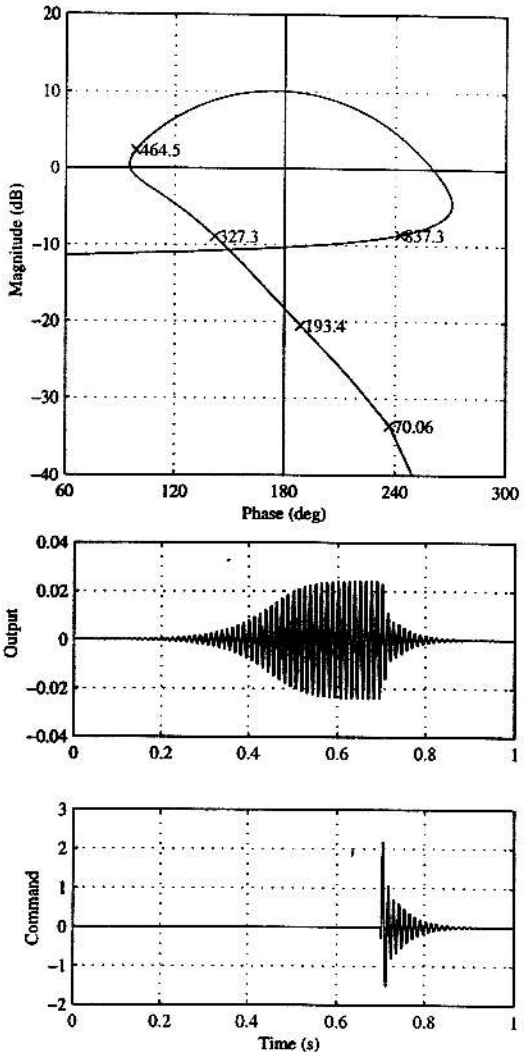

Figure 22 - Control function G_2. Black locus of LG_2C ; output and buffet suppression signals..

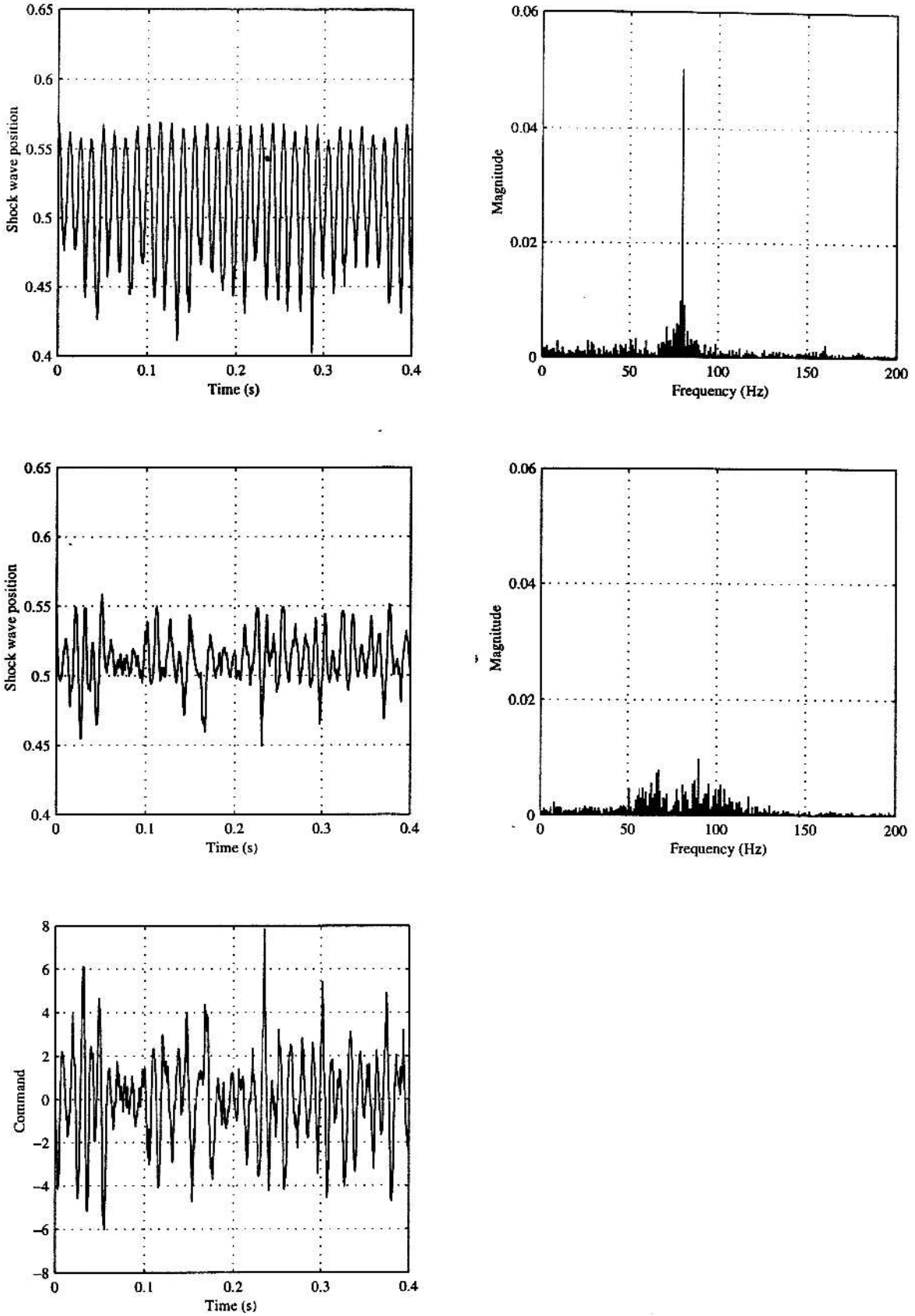

Figure 23 – Measured output signal without and with the buffet suppression control G_2 ; and the spectrum analysis of this signal.

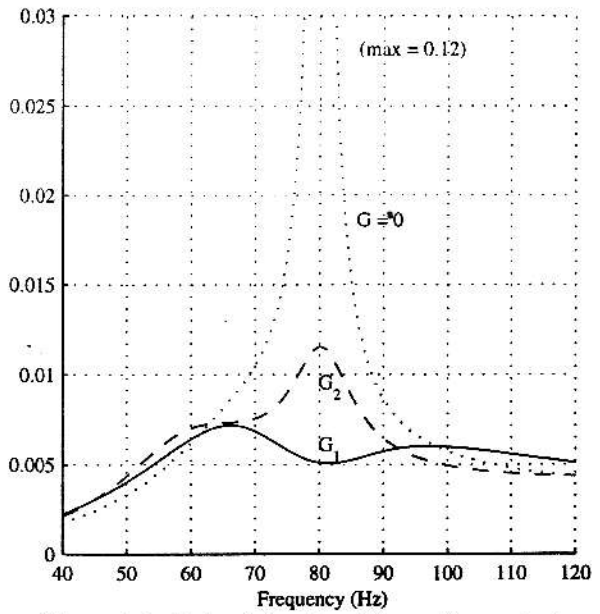

Figure 24 - Gain of the closed loop when output amplitude is equal to 0.02.

BIBLIOGRAPHY

[1] A. LE POURHIET, *Contribution à l'étude des oscillations forcées dans les asservissements par plus-ou-moins.* Thèse de maîtrise, février 1969, Université Laval, Québec.

[2] A. LE POURHIET, J.F. LE MAITRE, *Une méthode générale d'étude de la stabilité d'un système non linéaire oscillant.* Int. J. Control 12, 281-288 - 1970.

[3] A. LE POURHIET, J.G. PAQUET, *Jump Phenomenon in a Van der Pol Oscillator.* Automatica, vol. 7, pp. 481-487, 1971.

[4] J. Ch. GILLE, P. DECAULNE, M. PELEGRIN, *Systèmes asservis non linéaires.* Dunod, 1975, Paris.

[5] J. Ch. GILLE, P. DECAULNE, M. PELEGRIN, *Méthodes modernes d'étude des systèmes asservis.* Dunod, Paris, 1967.

[6] J.J. STOKER *Nonlinear vibrations,* pp. 147-187, Interscience, New York, 1966

[7] N. MINORSKY, *Introduction to non-linear mechanics,* pp. 341-354, J.W. Edwards, Ann Arbor, Mich., 1947.

[8] W.J. CUNNINGHAM, *Introduction to nonlinear analysis,* pp. 213-220, Mc Graw-Hill, New York, 1958

[9] L. SIDERIADES, *Les solutions forcées de l'équation de Van der Pol,* L'Onde Électrique, tome 45, n°3, octobre 1965, pp.1216-1224.

[10] C. HAYASHI, *Non-linear oscillations in physical systems,* MacGraw-Hill, New York, 1964.

[11] G. CHAPPAZ, *Aspects analytiques et analogiques des solutions de l'équation de Van der Pol en régime forcé sinusoïdal,* Int. J. nonlinear Mech. 3, 245-269, 1968.

[12] A. ANDRONOV, A. WITT, *Zur theorie des mitnehmens von Van der Pol,* Arch für Elektrotech, 1930.

[13] R. CHALEAT, *Sur l'équation de Lord Rayleigh,* Colloques internationaux du C.N.R.S., n°148, Éditions du C.N.R.S., p. 287, 1965.

[14] M.L. CARTWRIGHT, *Forced oscillations in nearly sinusoïdal systems,* J. Inst. Elec. Eng. (London) 95(3), 88-96, 1948.

[15] A.W. GILLIES, *On the transformation of singularities and limit cycles of the variational equation of Van der Pol,* Q.J. Mech. Appl. Math. 7, part 2, 1954.

[16] E.M. DEWAN, *Harmonic entrainment of Van der Pol Oscillations : Phaselocking and asynchronous quenching,* IEEE Transactions on Automatic Control, vol. AC 17, n°5, octobre 1972.

[17] A. LE POURHIET, *Comments on « Harmonic entrainment of Van der Pol Oscillations...»,* IEEE Transactions on Automatic Control, vol. AC-18, n°4, August 1973, pp. 412-414.

[18] D. CARUANA et al, *Contrôle actif des instabilités aérodynamiques à l'origine du tremblement,* Rapport ONERA RF 1/5700.05 DMAE, dec. 1998.

[19] D. CARUANA et al., *Contrôle actif des instabilités aérodynamiques à l'origine du tremblement. Ecoulement transsonique bidimensionnel. Phase 2,* Rapport ONERA RF 1/5700.10, DMAE, june 1999.

[20] C. DESPRÉ et al., *Buffet active control : experimental and numerical results,* Symposium RTO, Active Control, Technology for enhanced performance operational capabilities of aircrafts, Braunschweig, May 2000.

[21] D. CARUANA et al., *Buffet and buffeting active control,* AIAA, Fluids 2000, 19-22 june 2000, Denver, Co.